B-doped Carbon Coating Improves the Electrochemical Performance of Electrode Materials for Li-ion Batteries

Cong Wang, Ziyang Guo, Wei Shen, Qunjie Xu, Haimei Liu, and Yonggang Wang**

An evolutionary modification approach, boron doped carbon coating, is initially used to improve the electrochemical properties of electrode materials of lithium-ion batteries, such as $Li_3V_2(PO_4)_3$, and demonstrates apparent and significant modification effects. Based on the precise analysis of X-ray photoemission spectroscopy results, Raman spectra, and electrochemical impedance spectroscopy results for various B-doped carbon coated $Li_3V_2(PO_4)_3$ samples, it is found that, among various B-doping types (B_4C, BC_3, BC_2O and BCO_2), the graphite-like BC_3 dopant species plays a huge role on improving the electronic conductivity and electrochemical activity of the carbon coated layer on $Li_3V_2(PO_4)_3$ surface. As a result, when compared with the bare carbon coated $Li_3V_2(PO_4)_3$, the electrochemical performances of the B-doped carbon coated $Li_3V_2(PO_4)_3$ electrode with a moderate doping amount are greatly improved. For example, when cycled under 1 C and 20 C in the potential range of 3.0–4.3 V, this sample shows an initial capacity of 122.5 and 118.4 mAh g^{-1}, respectively; after 200 cycles, nearly 100% of the initial capacity is retained. Moreover, the modification effects of B-doped carbon coating approach are further validated on $Li_4Ti_5O_{12}$ anode material.

1. Introduction

Surface carbon coating is a low cost and high-efficiency modification approach in the field of lithium-ion battery electrode materials.[1–3] Compared with other kinds of surface coating methods, carbon coating has multi-functional advantages: the carbon layer can uniformly adhere to the surface of electrode and restrict the particle-size growth of electrode material; it also can effectively increase the electronic conductivity, avoid the direct contact with the electrolyte and improve the surface chemistry of the active material.[1] As a result, the electrochemical properties of the electrode materials with a thin outlayer of carbon are obviously improved, particularly for some electrode materials with very low electronic conductivity, such as $LiFePO_4$, $Li_3V_2(PO_4)_3$ and $Li_4Ti_5O_{12}$, and so on,[4–8] and therefore, surface carbon coating is indispensible and has got a wide range of applications. Wang et al. successfully synthesized uniform core–shell $LiFePO_4$/carbon particles and $Li_4Ti_5O_{12}$/C materials via an in situ polymerization restriction method,[4,8] both of these two electrodes show excellent cycling performance and rate performance after carbon coating modification. Mao et al. prepared an uniform carbon coated $Li_3V_2(PO_4)_3$ composite via an in situ polymerization method, this $Li_3V_2(PO_4)_3$/C also shows good cycle stability and high rate performance.[6]

As the above, an important aim of carbon coating is to improve the electric conductivity and increase the electrochemical stability and activity of electrode materials. Generally, the precursors for carbon coating are organic compounds, and then by high temperature calcinations-carbonation process to form a coated carbon layer. However, for most of electrode materials of LIBs, the synthesis temperatures are always under 1000 °C, and at this temperature, carbon cannot be completely graphitized, therefore, the conductivity of the carbon layer is low. On the other hand, to increase the synthesis temperature is an effective way to enhance the conductivity of the carbon layer, but will cause thermal carbon reduction, also is the loss of oxygen. Therefore, how to further increase the conductivity of the carbon coating layer without increasing the synthesis temperature, it is still a grand challenge. At present, non-metallic elements doping, such as nitrogen doping and boron doping etc.,[9–14] are widely used to improve the electric properties of carbon-based materials and also exhibits excellent modification effects. However, there are rare studies focused on the modification effects of heteroatom doping on the surface carbon coated layer, furthermore, there are few works combined the heteroatom doping in carbon coating method and jointly used to bedeck the electrode materials. Recently, it is noticed that nitrogen-doped carbon coating approach has occasionally been used to embellish the electrode materials, such as $Li_4Ti_5O_{12}$, $LiFePO_4$ and $Li_3V_2(PO_4)_3$;[15–17] and reflected obvious modification effects. However, there are rare reports to explain in-depth how N-doping can further impact

Prof. Q. Xu, Prof. H. M. Liu
College of Environmental and Chemical Engineering
Shanghai University of Electric Power
Shanghai 200090, China
E-mail: liuhm@shiep.edu.cn
C. Wang, W. Shen, Prof. H. M. Liu
State Key Laboratory of Chemical Resource Engineering
Beijing University of Chemical Technology
Beijing 100029, China
Z. Guo, Prof. Y. G. Wang
Department of Chemistry and Shanghai Key Laboratory of Molecular Catalysis and Innovative Materials
Institute of New Energy
Fudan University
Shanghai 200433, China
E-mail: ygwang@fudan.edu.cn

DOI: 10.1002/adfm.201401006

© 2014 WILEY-VCH Verlag GmbH & Co. KGaA, Weinheim

the modification effects of carbon coating and which N-doped type causes this modification effects on the carbon coating layer so far.

Similarly, boron doping, identical to nitrogen doping, also is the essential modified approach of carbon-based materials,[11,14,18] because B-doping could bring many amazing improvements on these carbon-based materials: firstly, B-doping could break the electroneutrality of carbon-based materials and create many active sites;[11] secondly, B-doping could change the electronic structure and enhance the electrical properties of carbon-based materials;[18,19] thirdly, the introduction of boron also increases the number of hole-type charge carriers, which enhance the conductivity of carbon materials obviously.[20] Therefore, in this report, we firstly adopt boron-doped carbon coating approach to modify the electrode materials of lithium ion batteries and explain in detail the causes of the modification effects. Consequently, $Li_3V_2(PO_4)_3$ cathode and $Li_4Ti_5O_{12}$ anode materials are selected as our target modified materials in this report to verify and expound the modification effects of B-doped carbon coating approach. In this research, it is worthwhile to be noted that with the increase of boron doping amount in carbon coating layer, the variation for the electrochemical properties of various boron doped carbon coated $Li_3V_2(PO_4)_3$ materials exhibit certain regularity. As a result, the relationship between the electrochemical performance of various B-doped carbon coated $Li_3V_2(PO_4)_3$ cathode materials and the doping types of boron in carbon-based materials was analyzed and explained in detail in this research. Based on the modification effects on $Li_3V_2(PO_4)_3$ and $Li_4Ti_5O_{12}$, we believe that moderate boron doped carbon coating is a concise and high-efficient approach for the electrode material which conductive material coating is indispensable.

2. Results and Discussion

2.1. Results

In order to verify and analyze the modification effect of B-doped carbon coating approach, boron-doped carbon coated $Li_3V_2(PO_4)_3$ and $Li_4Ti_5O_{12}$ (referred as LVP/C+B and $Li_4Ti_5O_{12}$/C+B, respectively) were synthesized. Wherein, critic acid and $NaBC_{24}H_{20}$ are used as carbon and boron source, and for preparation of LVP/C+B composites with different B concentration, $NaBC_{24}H_{20}$ was added with different molar ratio to critic acid of 0, 0.33, 0.50, 0.67 and 0.83%, respectively. In the following, for simplicity, above-mentioned LVP/C+B composites with various boron contents are marked as LVP/C, LVPC-B33, LVPC-B50, etc., (details see experimental section). Typical X-ray diffractions (XRD) of the as-fabricated B-doped carbon coated $Li_3V_2(PO_4)_3$ samples together with the only carbon coated $Li_3V_2(PO_4)_3$ are displayed in **Figure 1**. It is obvious that there is nearly no difference between LVP/C and various LVP/C+B samples, all of the diffraction peaks can be assigned to the monoclinic $Li_3V_2(PO_4)_3$ (S.G. $P2_1/n$) with the lattice parameters a-8.606 Å, b-8.592 Å, c-12.037 Å, and β-90.61°, in good agreement with the JCFDS card No. 01–072–7074. It is noticed that because the excess of Li source in raw materials and the loss of V in subsequent heat treatment process, a small amount of Li_3PO_4 impurity phase

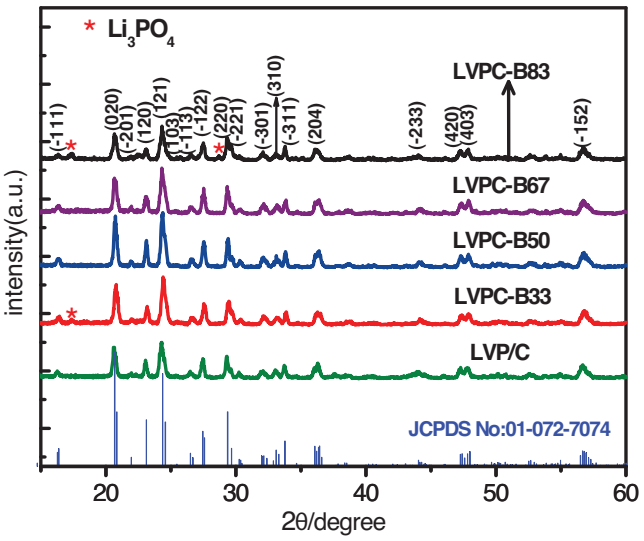

Figure 1. XRD patterns of LVP/C and various LVP/C+B samples.

is observed in the LVPC-B33 and LVPC-B83 samples.[21] These XRD patterns indicate that the boron-doped into carbon layer does not affect the structure of the $Li_3V_2(PO_4)_3$ material. Furthermore, the carbon contents of various $Li_3V_2(PO_4)_3$ composites in this report have been measured by the organic element analyzer. The carbon content of LVP/C, LVPC-B33, LVPC-B50, LVPC-B67, LVPC-B83 is 4.61%, 4.37%, 4.13%, 4.00% and 3.88%, respectively. It is noticed that the carbon contents of LVP/C and various LVP/C+B samples are very close to each other, that is to say, different B doping degrees in carbon coated $Li_3V_2(PO_4)_3$ composites do not make obvious distinction on the carbon contents of various samples.

In order to supply sufficient evidence to confirm the successful doping of boron in the carbon layer on $Li_3V_2(PO_4)_3$, the detailed X-ray photoemission spectroscopy (XPS) of LVP/C and various LVP/C+B samples were carried out. Moreover, based on the atom percents (At%) of carbon and boron in XPS data as well as the carbon contents of various LVP/C+B samples, the specific concentrations of boron in various LVP/C+B have been calculated, and the actual percentage composition of boron in LVPC-B33, LVPC-B50, LVPC-B67 and LVPC-B83 is 0.251%, 0.387%, 0.422% and 0.503%, respectively. **Figure 2** shows the typical high resolution XPS spectra of C1s for LVP/C and various LVP/C+B samples, it is observed in Figure 2a that with the increase of the B amount in carbon layer, the C1s peak broadens gradually, of which may be attributed to the introduction of B–C, O–B–C and C–O species.[22] In all the detailed XPS spectra of C1s for LVP/C and various LVP/C+B samples, which displayed in Figure 2b–f, the peaks at binding energies of 284.6 and 286.8 eV can be attributed to sp^2 graphite C=C bonds and C–O bonds.[22–24] However, compared with the C1s spectra of LVP/C in Figure 2b, an obvious peak at ~283.5 eV,[25,26] which can be assigned to the C–B species, is clearly observed in C1s spectra for all LVP/C+B samples as exhibited in Figure 2c–f. Moreover, with the gradually increase of the B dopant, the peak area of the B–C species shows the similar increase tendency, therefore, demonstrating the formation of B–C bond in the carbon layer on various LVP/C+B samples. Besides, the

© 2014 WILEY-VCH Verlag GmbH & Co. KGaA, Weinheim

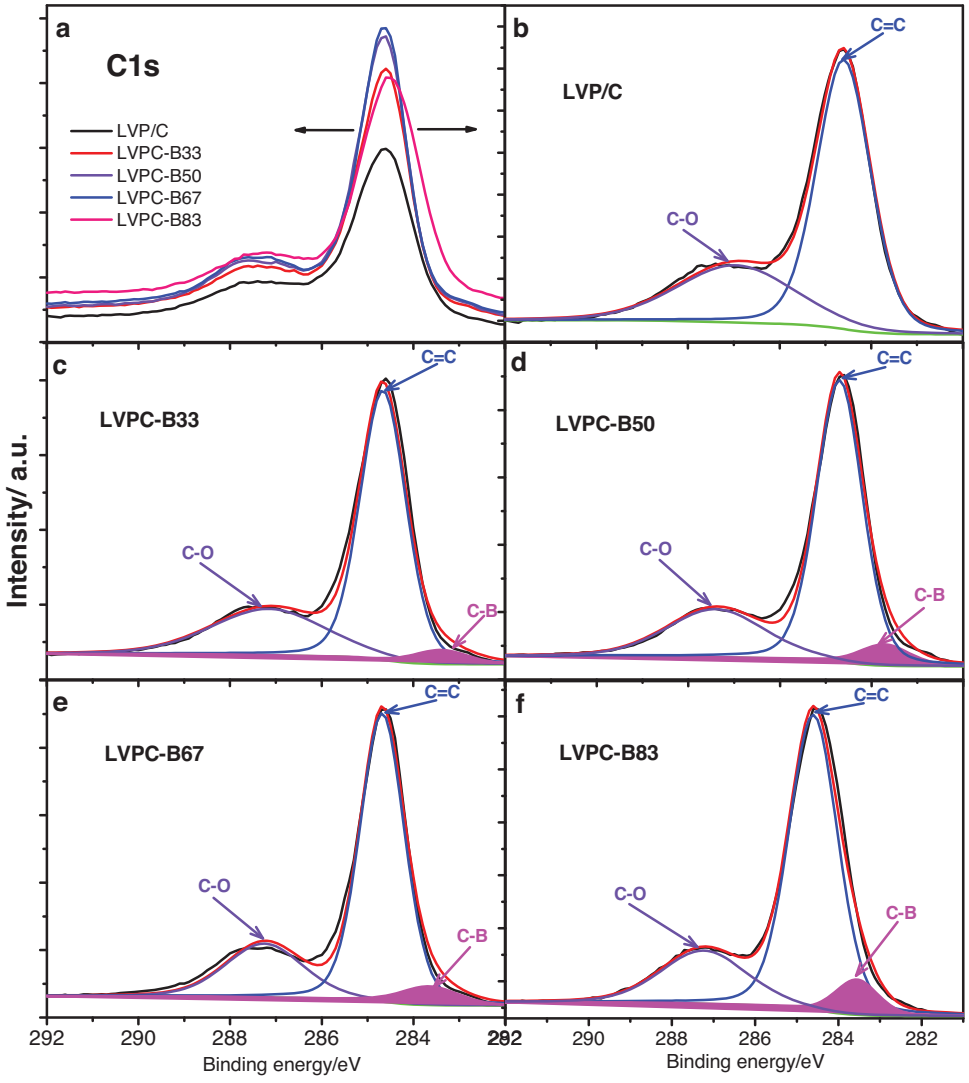

Figure 2. High-resolution XPS spectra of b) LVP/C and c–f) various LVP/C+B samples on C1s.

variation and differences of the peak area at 532.5 eV in O1s spectra, which attributed to the C–O and B–O species, also indicate the existence of boron on doped samples (Supporting Information, Figure S1). Furthermore, the B element mapping of LVPC-B50, as clearly observed in Figure S2, reveals that boron is homogenously distributed in the surface carbon layer of $Li_3V_2(PO_4)_3$.

The above-mentioned argument for boron doping in the carbon coated layer is further supported by the high-resolution XPS spectra of various LVP/C+B samples on B1s. As is shown in **Figure 3**, the B1s spectra of various LVP/C+B samples are all divided into four components: the peak at the lowest bonding energy ~187.5 eV is assigned to B_4C type bond,[27] the peak at ~189.5 eV is attributed to BC_3 type bond,[11,27,28] the peaks centered at ~190.8 eV and ~192.7 eV are correspond to the BC_2O and BCO_2 type bonds, respectively.[11,23,27,29] It can be clearly observed that the distribution and contents of various B-C bond types among various LVP/C+B samples are different. The variation in the amount of various B–C bonds is critical and may influence the electrochemical properties of various LVP/C+B samples. In addition, there is no difference between the P2p XPS spectra of LVP/C and LVPC-B50 (Supporting Information, Figure S3), which further indicates that boron is only doped into the surface carbon layer and makes no effect on the crystal structure of $Li_3V_2(PO_4)_3$ (Figure 1).

In order to observe and validate the influence of the boron doping amount on the electrochemical properties of various samples, the electrochemical performances of LVP/C and various LVP/C+B are investigated in detail. **Figure 4**a–f show the initial charge-discharge profiles and cycling stabilities of LVP/C and various LVP/C+B samples at the current densities of 1 C (1 C = 133 mA g^{-1}, 3–4.3 V), 10 C and 20 C in the potential range of 3.0–4.3 V *vs.* Li/Li^+. As seen in Figure 4a, all of LVP/C and various LVP/C+B samples exhibit three charge and discharge plateaus, of which have been well identified as two phase transitions during the charge and discharge process,[30,31] and with the increase of current density (seen in Figure 4c and e), an obvious potential drop is observed and the discharge platforms

© 2014 WILEY-VCH Verlag GmbH & Co. KGaA, Weinheim

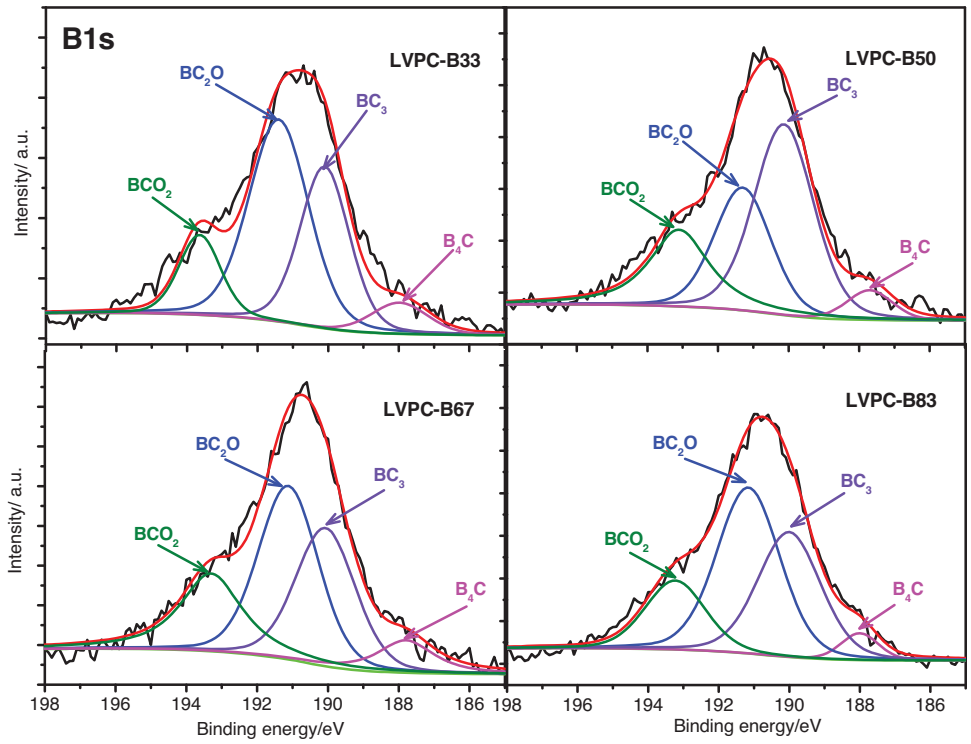

Figure 3. High-resolution XPS spectra of various LVP/C+B samples on B1s.

become unclear, which is owing to the electrode polarization. Among the various $Li_3V_2(PO_4)_3$ samples, LVPC-B50 shows the highest initial discharge capacity, capacities of 122.5, 122.3 and 118.6 mAh g^{-1} can be achieved at 1 C, 10 C and 20 C, and still maintain at 121.2, 121.2 and 118.1 mAh g^{-1} after 200 cycles, respectively (seen in Figure 4b, d and f). As for the controlled LVP/C, its initial discharge capacities at 1 C, 10 C and 20 C are 100.8, 94.5 and 92.7 mAh g^{-1}, respectively; and maintain at 99.7, 91.5 and 94.4 mAh g^{-1} after 200 cycles, respectively. It is found that under all current densities, generally, the cycling stability of LVPC-B50 is better than that of LVP/C and other LVP/C+B samples. It also can be seen in Figure S4 that LVPC-B50 shows the best rate stability among all the LVP/C+B samples in the potential range of 3.0–4.3 V vs. Li/Li^+: after cycling at 30 C, its discharge capacity can still reach 123.5 mAh g^{-1} when re-cycled at 1 C. Figure 4g presents initial charge–discharge profiles in the potential range of 3.0–4.8 V vs. Li/Li^+ at 0.2 C (1 C = 197 mA g^{-1}, 3–4.8 V), for all samples, all three of the Li^+ can be extracted and four charge plateaus are observed during the charge process but three plateaus are exhibited in the discharge process between 3.0–4.8 V,[30,31] the initial capacities of the LVP/C, LVPC-B33, LVPC-B50, LVPC-B67 and LVPC-B83 are 136.2, 130.9, 169.6, 157.5 and 126.4 mAh g^{-1}, respectively. The cycle performances in the potential range of 3.0–4.8 V as displayed in Figure 4h, LVPC-B50 shows the highest discharge capacity and the best cycling property. It is also found in Figure 4i and Figure S5, LVPC-B50 demonstrates an excellent cycling stability and rate performance in this high potential range of 3.0–4.8 V vs. Li/Li^+ under various current densities. It is noteworthy that, compared with LVP/C, the electrochemical performances of various LVP/C+B samples meliorate initially and then deteriorate with the increase of the boron doping amount. Furthermore, no matter under various current densities or in various potential ranges, the electrochemical properties of various LVP/C+B samples exhibit same varying pattern. Therefore, boron-doped carbon layer on $Li_3V_2(PO_4)_3$ makes significantly positive effects on its electrochemical properties when B-doping amount is moderate and optical, and the reasons will be analyzed and discussed in detail in the following section.

2.2. Discussion

In this work, $Li_3V_2(PO_4)_3$ cathode materials are coated by a boron-doped carbon layer and the modification effect is prominent and apparent, thereby, it is quite necessary to make a close observation on the carbon coated layer of LVP/C and LVP/C+B samples. **Figure 5** shows the HRTEM images of LVPC-B50 and LVP/C, it is noticeable in Figure 5a and c that a homogeneous and uniform carbon layer is formed on LVPC-B50 and LVP/C surface, and the selected area electron diffraction (SAED) patterns in inset indicate the high crystallization character of both of two samples, and the marked lattice fringes with *d*-spacing of 0.202 and 0.204 nm, which clearly observed in Figure 5a, b and c, corresponding to the (120) and (-111) planes of the monoclinic $Li_3V_2(PO_4)_3$. The thickness of the carbon layer on both of LVPC-B50 and LVP/C is around 3~7 nm, and more interestingly is that in some selected areas (Figure 5b), there are somewhat graphite-like carbon with the layered structures of ~0.34 nm in the carbon layer observed apparently.[21] Therefore, it seems that based on the above observation, the complete and

© 2014 WILEY-VCH Verlag GmbH & Co. KGaA, Weinheim

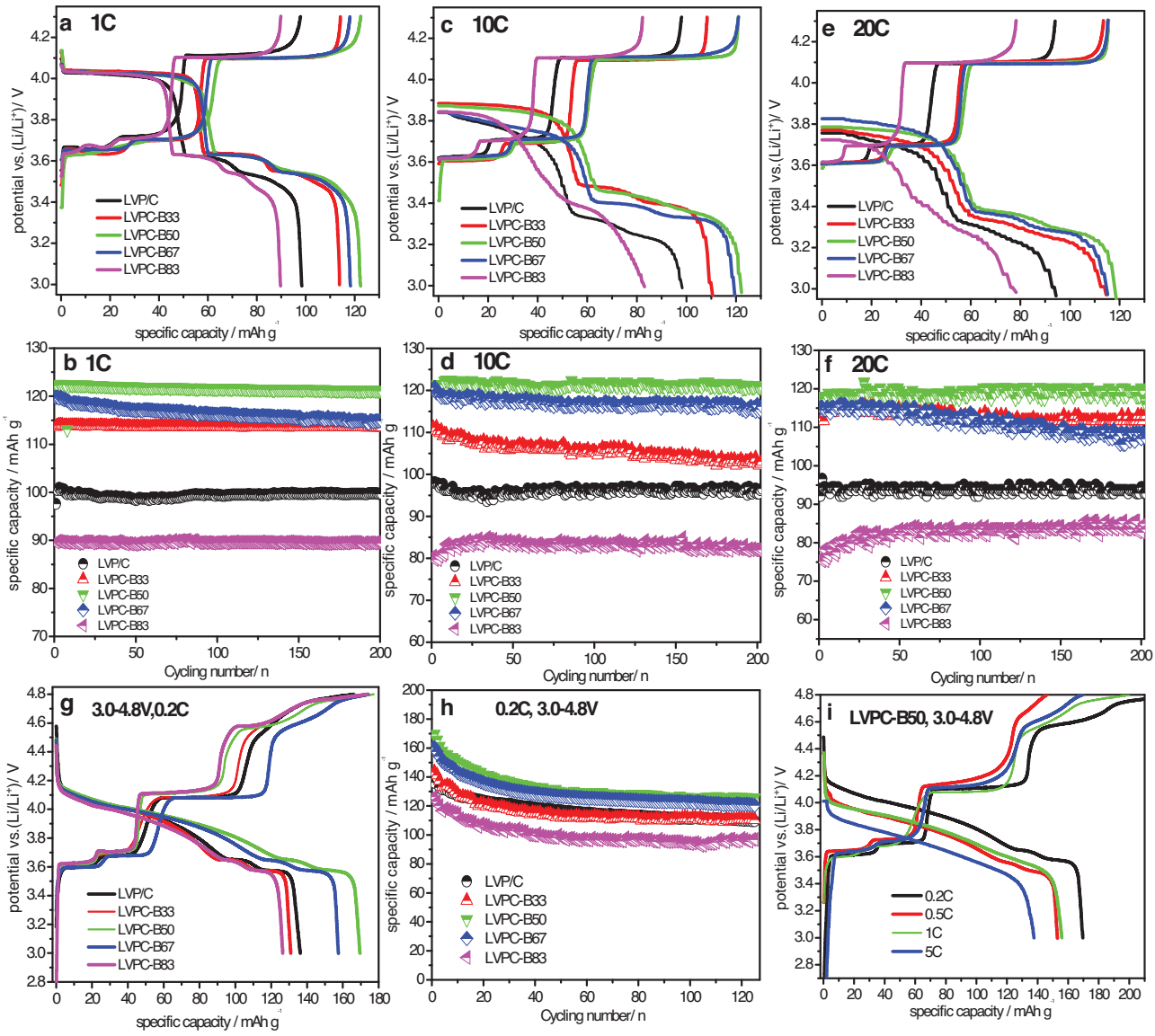

Figure 4. Initial charge–discharge curves and cycling performances of LVP/C and various LVP/C+B samples in the potential range of 3.0–4.3 V at various current densities: a) and b) 1 C, c) and d) 10 C, e) and f) 20 C; g) initial charge–discharge curves and h) cycling performances of LVP/C and various LVP/C+B samples in the potential range of 3.0–4.8 V at 0.2 C; i) initial charge-discharge curves of LVPC-B50 in the potential range of 3.0–4.8 V at various current densities.

uniform surface carbon layer may be the origin for significantly improved electrochemical properties of LVPC-B50. However, as shown in the HRTEM images, there is nearly no obvious difference in the integrity of coated carbon layer and degree of crystallinity between LVPC-B50 and LVP/C samples. Thus, it is quite reasonable to anticipate that the differences of electronic structure and electrical properties on the coated carbon layer, which were induced by boron doping, may be the most essential reason for the distinction of the electrochemical performances among various $Li_3V_2(PO_4)_3$ samples. Hereinafter, this reason will be analyzed and discussed thoroughly.

Based on the analysis of B1s high-resolution XPS spectra of various LVP/C+B samples in Figure 3, there are four B doped types appeared in all LVP/C+B samples, but the distribution of various B doped types in various LVP/C+B samples is totally different. **Figure 6** demonstrates the distribution of B_4C, BC_3, BC_2O and BCO_2 in various LVP/C+B samples. As shown in Figure 6a and Figure S6, compared with another three B types, the ratios of the B_4C doped type in various LVP/C+B samples are all relatively low and this binding of B_4C is accompanied by defects inside the carbon coated layer network.[32] However, due to the low content of B_4C, this doped type makes little influence on the electrochemical performance of various LVP/C+B samples. Figure 6b displays the percentage of the BC_3 in each LVP/C+B samples, with the increase of B doping amount in LVP/C+B, the percentage of the BC_3 climb up and then decline, which has the same varying pattern with the electrochemical properties of various LVP/C+B samples. Therefore,

© 2014 WILEY-VCH Verlag GmbH & Co. KGaA, Weinheim

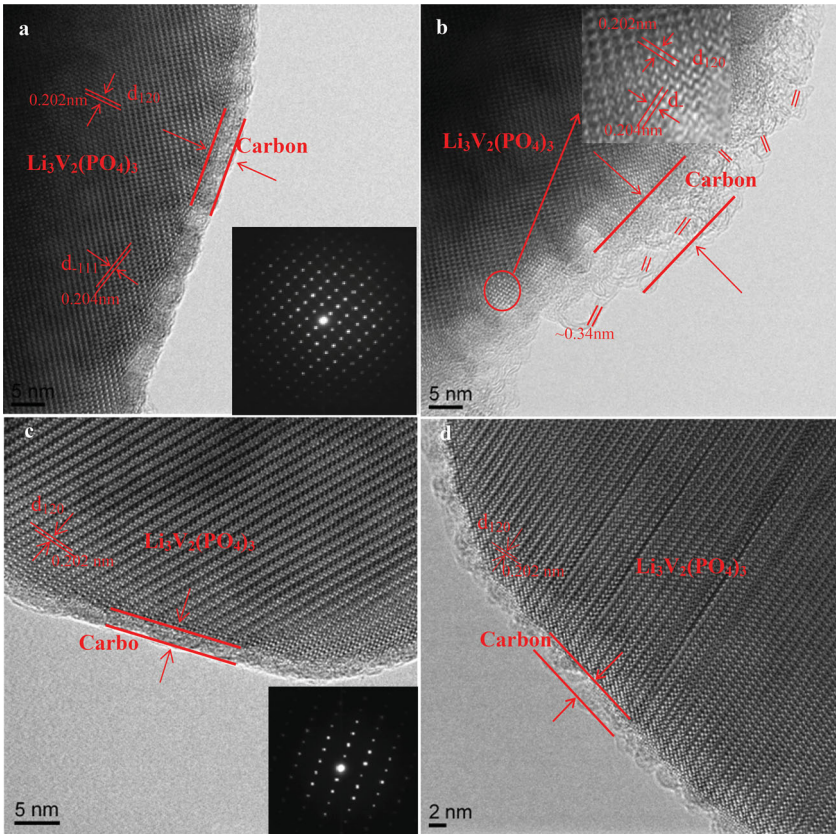

Figure 5. HRTEM imagines of a) and b) LVPC-B50 and c) and d) LVP/C, inset in a) and c): the corresponding SAED patterns.

BC_3 doped type in the carbon coated layer should play a huge role on the improvement of the electrochemical performance of LVP/C+B samples. On the one hand, the graphite-like BC_3 doped type plays an important role in changing the valence band structure of carbon-based materials and increasing the density of states near the Fermi level,[32,33] which could improve the electronic conductivity of LVP/C+B samples; on the other hand, the introduction of boron in carbon layer, such as BC_3 doped type, increases the number of hole-type charge carriers and also increases the electron density on nearby active carbon sites,[20,22] which enhances the conductivity and electrochemical activity of LVP/C+B surface carbon coated layer. However, because boron preferred bond with oxygen elements to bond with carbon elements, as displayed in Figure 6c and d, the percentage of the BC_2O and BCO_2 doped types, especially BC_2O, increased obviously with the increase of B doped amount in LVP/C+B samples. The emergence of BC_2O and BCO_2 doped types indicates the boron doping positions are on the edge of the carbon coated layer and these two B doped types, particularly BCO_2, may make negative effects on the electrochemical performance of various LVP/C+B samples. Based on the above analysis, the distribution of various B doped types, especially of the BC_3, induces the distinction and varying pattern of the electrochemical performances of various LVP/C+B samples.

The above argument was further supported strongly by the electronic conductivities investigations of various LVP samples measured at the pressure of 4 MPa by a 4-pole conductivity instrument for power materials. As shown in **Table 1**, the electronic conductivity of the LVPC-B50 powder reaches 69.77S/cm, which is more than 3488 times higher than that of the LVP/C powder, which exhibits the best electronic conductivity among the five power materials. Herein, it should be reminded that, as discussed earlier, the graphite-like BC_3 plays a key role in enhancing the electronic conductivity of the materials, and exactly the LVPC-B50 has the highest percentage of this dopant component (Figure 6). Therefore, all these observations seem reasonable and easily understand that LVPC-B50 demonstrates the highest electronic conductivity and the best electrochemical property (Figure 4). Furthermore, the electronic conductivity of the LVPC-B33 is close to the LVPC-B67, and is slightly higher than that of the LVPC-B83 powder, exhibiting a good agreement with their electrochemical performances in the Figure 4.

In order to further observe the difference of the defect level in the carbon coated layers of various $Li_3V_2(PO_4)_3$ samples, Raman spectra of LVP/C and various LVP/C+B samples are tested. It is distinctly indicated in **Figure 7** that the Raman spectra of all samples show two prominent peaks of D band and G band as well as a very weak 2D band. The intensity of the D band is closely associated with the disorder degree of carbon materials, while the G band is attributed to the first order scattering of the stretching vibration mode E_{2g} observed for the sp^2 carbon domain.[12] Generally, the value of the intensity ratio of D band to G band (I_D/I_G) is used to estimate the degree of disorder and defects of carbon materials.[34,35] As shown in the inner of Figure 7, the values of I_D/I_G for LVP/C, LVPC-B33, LVPC-B50, LVPC-B67 and LVPC-B83 are 1.025, 1.040, 1.063, 1.061 and 1.032, respectively. It is noteworthy that all LVP/C+B samples have higher value of I_D/I_G than that of LVP/C, which means more defects are existed in the surface carbon coated layer of LVP/C+B samples. Based on the previous reports,[12,36] the topological defects produced during the boron doping process may enable the doped carbon coated layer to be favorable for Li^+ pass through and storage, consequently further improve the electrochemical performance of $Li_3V_2(PO_4)_3$ cathode material.

Table 1. Powder electronic conductivities of LVPC-B33, LVPC-B50, LVPC-B67, LVPC-B83 and LVP/C powders measured at a pressure of 4 MPa.

Material	Conductivity [S/cm]
LVPC-B33	16.26
LVPC-B50	69.77
LVPC-B67	12.05
LVPC-B83	1.69
LVP/C	0.02

© 2014 WILEY-VCH Verlag GmbH & Co. KGaA, Weinheim

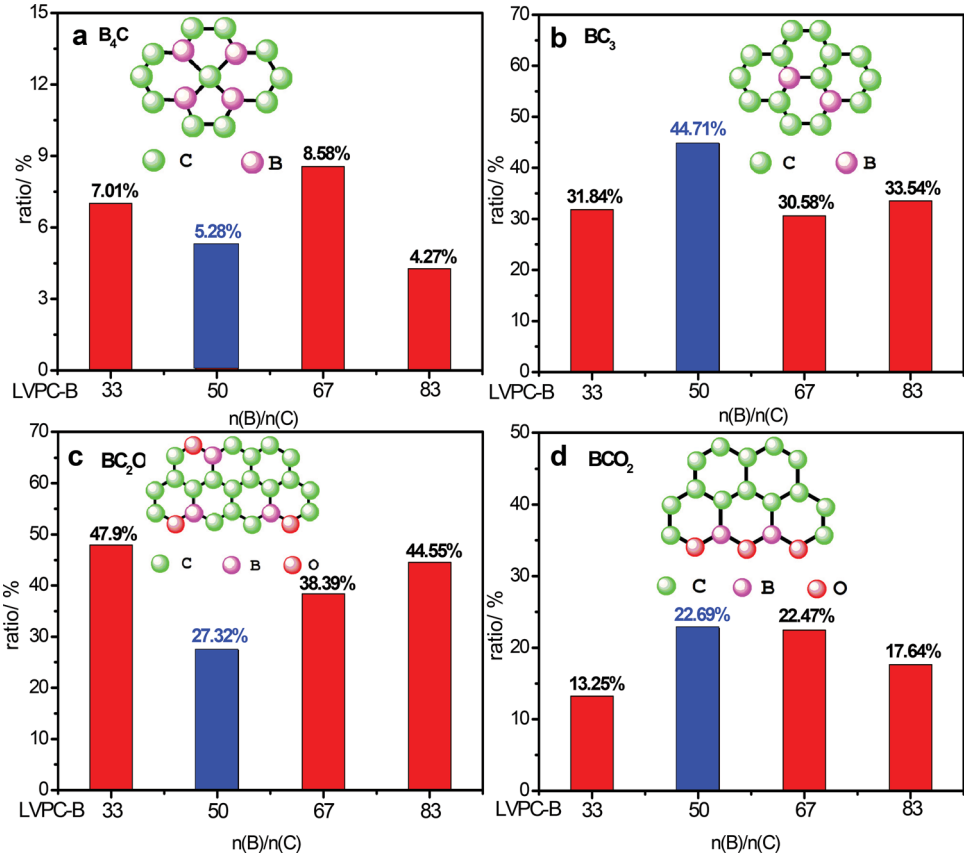

Figure 6. The ratio and model of different B types in various LVP/C+B samples: a) B_4C, b) BC_3, c) BC_2O and d) BCO_2.

To verify and investigate the positive effect of boron doped carbon coating on the electronic conductivity and electrochemical kinetics of $Li_3V_2(PO_4)_3$, electrochemical impedance spectroscopy (EIS) tests of LVP/C and various LVP/C+B samples are carried out. The EIS tests are conducted in the frequency range of 1 MHz to 10 mHz at the full charge state (4.3 V) after 50 and 100 cycles, and the corresponding three-dimensional Nyquist plots of various $Li_3V_2(PO_4)_3$ samples are displayed in **Figure 8**a and b. It is obviously noted that, whether after 50 or 100 cycles, the shapes of the Nyquist plots for various $Li_3V_2(PO_4)_3$ samples are similar. Figure 8c presents an equivalent circuit to simulate the electrochemical impedance spectroscopy data. In the equivalent circuit: R_1 (R_s) represents the resistance of electrolyte, electrode and separator, which corresponds to the intercept at high frequency; R_2 (R_{SEI}) and CPE1 are the resistance and capacitance of the surface film formed on the electrode, respectively, which correspond to the semicircle at high frequency region; R_3 (R_{ct}) and CPE2 are the charge transfer resistance and double layer capacitance, respectively, which correspond to the semicircle in the high medium frequency region; the W_1 represents the warburg impedance related to the diffusion of lithium ions into the bulk electrode which corresponds to the slope line in the low frequency region. The fitting values from this equivalent circuit of various $Li_3V_2(PO_4)_3$ samples after 50 and 100 cycles are listed in **Table 2**. As it can be seen in the table, whether after 50 or 100 cycles, R_1 (R_s) and R_2 (R_{SEI}) are similar for all samples, and their values, especially R_1 (R_s) is relatively low compared to R_{ct}. It can be expressly noted that, after 50 cycles, the charge transfer

Table 2. The impedance value of LVP/C sample and various LVP/C+B samples after 50th and100th cycles.

Impedance*	LVPC-B 33	LVPC-B 50	LVPC-B 67	LVPC-B 83	LVP/C	
$R_1(R_s)$ [Ω]	50th	2.18	1.96	1.77	1.67	1.94
	100th	2.87	1.72	1.96	2.53	1.93
$R_2(R_{SEI})$ [Ω]	50th	41.5	23.18	30.71	41.94	28.84
	100th	21.1	10.64	10.74	11.94	8.84
$R_3(R_{ct})$ [Ω]	50th	138.8	45.09	53.42	271.4	192.8
	100th	194.1	69.96	82.94	278.6	248.4

*The EIS measurements of all samples are all carried out in the frequency range of 1 MHz to 10 mHz at the charge state (4.3 V) after 50th and 100th cycles.

© 2014 WILEY-VCH Verlag GmbH & Co. KGaA, Weinheim

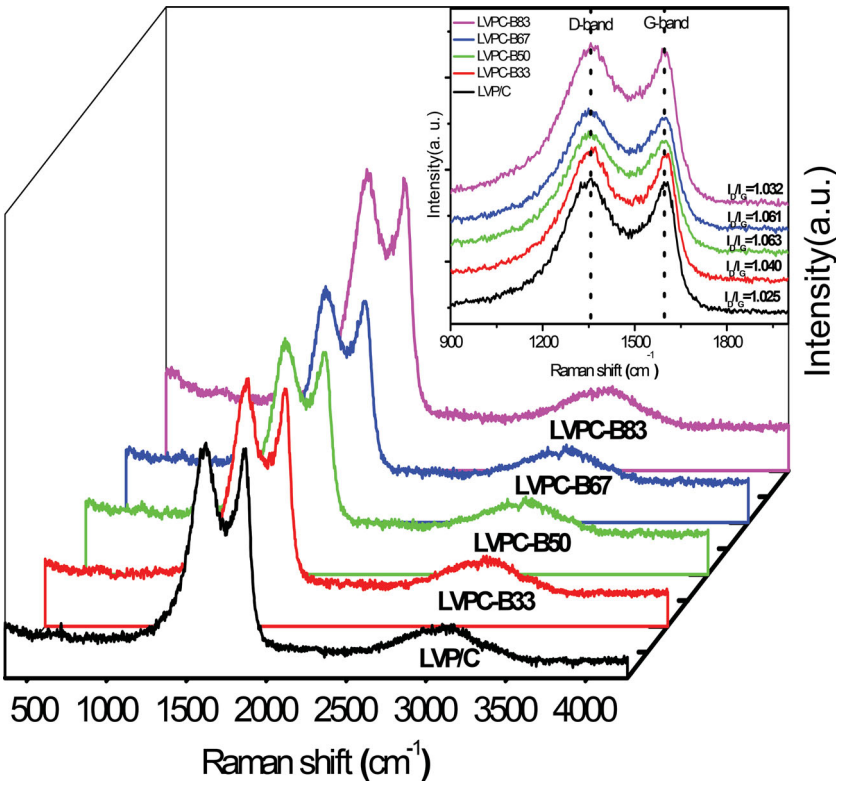

Figure 7. Raman spectra of LVP/C and various LVP/C+B samples.

resitance (R_{ct}) value are 138.8, 45.09, 53.42, 271.4 and 192.8 Ω; and after 100 cycles, the value increased to 194.1, 69.96, 82.94, 278.6 and 248.4 Ω for LVPC-B33, LVPC-B50, LVPC-B67, LVPC-B83 and LVP/C, respectively. It is noticed that the LVPC-B50 exhibits the lowest value of R_{ct}, which indicates that moderate doping amount can effectively improve the electronic conductivity and enhance the insertion/exertion behavior of lithium-ion in the $Li_3V_2(PO_4)_3$ surface carbon coated layer. Based on the analysis results of the EIS test and Raman spectra, when B doping amount in the carbon coated layer is moderate, B-doped carbon coating indeed makes powerful and positive effects on the electrochemical properties of $Li_3V_2(PO_4)_3$ cathode material.

With the aim to certify the modification effects of this B-doped carbon coating is not occasional, another target material – $Li_4Ti_5O_{12}$, is also modified by boron doped carbon coating, and its electrochemical properties are compared with $Li_4Ti_5O_{12}$/C in detail. As shown XRD patterns in Figure S7a, for $Li_4Ti_5O_{12}$/C+B and $Li_4Ti_5O_{12}$/C samples, the observed diffraction peaks can be well indexed to spinel $Li_4Ti_5O_{12}$ (JCPDS file No. 26–1198),[37,38] which means B-doped carbon coating does not affect the structure of $Li_4Ti_5O_{12}$. It is noticed that because of the long sintered time and high temperature, a small amount of rutile TiO_2 is observed, which also causes the slope in discharge curves shown in Figure S7b. **Figure 9**a displays the overall rate capability test of $Li_4Ti_5O_{12}$/C+B and $Li_4Ti_5O_{12}$/C from 0.5 C to 30 C (1 C = 170 mA g^{-1}, 1.0–3.0 V *vs.* Li/Li$^+$), it is noteworthy that $Li_4Ti_5O_{12}$/C+B shows bettter rate stability than that of $Li_4Ti_5O_{12}$/C sample. Figure 9b and Figure S7b present the cycling performance and initial charge–discharge curves of $Li_4Ti_5O_{12}$/C+B and $Li_4Ti_5O_{12}$/C at 1 C (1 C = 170 mA g^{-1}, 1.0–3.0 V), the initial capacities of $Li_4Ti_5O_{12}$/C+B and $Li_4Ti_5O_{12}$/C are 142.7 and 133.3 mAh g^{-1}; and when cycled to 200 cycles, the specific capacities are stabilized at 134.6 and 121.8 mAh g^{-1}, resperctively, which means the cycling

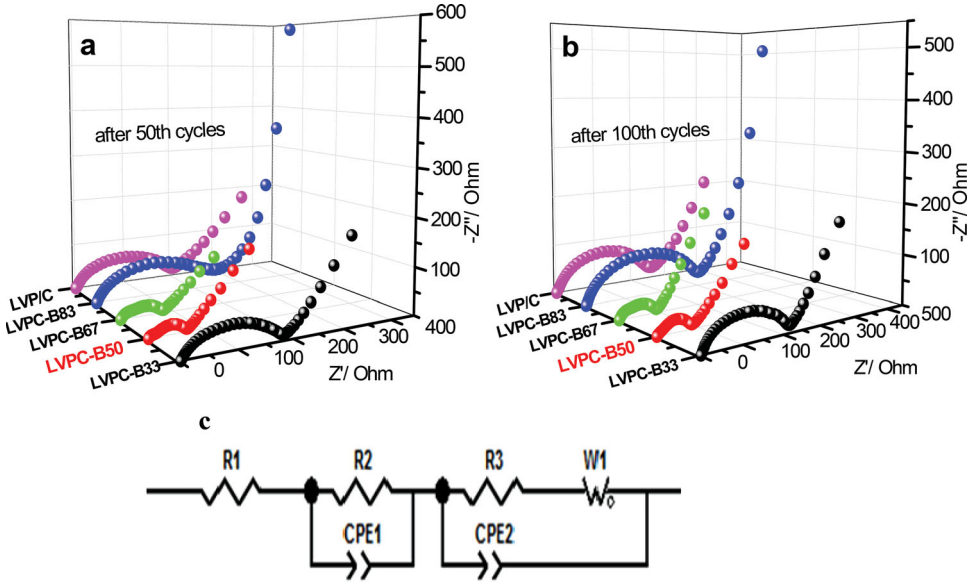

Figure 8. Nyquist plots of LVP/C and various LVP/C+B samples after a) 50th cycle and b) 100th cycle at a full charge state (4.3 V); c) equivalent circuit used for simulating the experimental impedance data.

© 2014 WILEY-VCH Verlag GmbH & Co. KGaA, Weinheim

performance of $Li_4Ti_5O_{12}$/C+B is better than that of $Li_4Ti_5O_{12}$/C. Compared with C1s XPS spectra of $Li_4Ti_5O_{12}$/C (Figure S8a), an obvious peak of C-B spaces at ~283.5 eV,[25,26] is clearly observed in C1s XPS spectra of $Li_4Ti_5O_{12}$/C+B (Figure S8b), which demonstrates B is successfully doped in carbon coated layer of $Li_4Ti_5O_{12}$/C+B. It can be clearly observed in Figure 9c that four B doped types: B_4C, BC_3, BC_2O and BCO_2 are also existed in the $Li_4Ti_5O_{12}$/C+B carbon coated layer. Figure 9d demonstrates the distribution of B_4C, BC_3, BC_2O and BCO_2 in $Li_4Ti_5O_{12}$/C+B: because B preferred bond with oxygen to bond with carbon elements, the doping amount of BC_2O is the most abundant. The percentage of BC_3 is 25.21%, this doped type plays a prominent role on improving the electronic conductivity of $Li_4Ti_5O_{12}$ surface carbon layer, as a result, makes positive effects on the electrochemical performances of $Li_4Ti_5O_{12}$. In a word, the modification effects of boron doped carbon coating are both embodied in $Li_3V_2(PO_4)_3$ and $Li_4Ti_5O_{12}$ electrode materials.

3. Conclusions

By using a convenient sol–gel method, the boron-doped carbon coating was initially adopted and used to bedeck LIBs electrode materials. In this work, after modified by boron-doped carbon coating with moderate amount, especially the existance of BC_3 dopant species, the electronic conductivity and electrochemical activity of the carbon layer on $Li_3V_2(PO_4)_3$ surface are greatly ameliorated. With the increase of boron doping amount, the electrochemical properties of the $Li_3V_2(PO_4)_3$ meliorate initially and then deteriorate, presenting a same variation trend with contents of BC_3 among various LVP/C+B samples. Furthermore, this B-doped carbon coating are further validated on $Li_4Ti_5O_{12}$ material, again demonstrating its effectiveness and significance. Thereby, it is believed that this modification approach of B-doped carbon coating is more effective than that of the bare carbon coating and may be widely applied to improve the electrochemical performance of LIBs electrode material, of which the conductive material coating is indispensable, such as $LiFePO_4$.

4. Experimental Section

Materials Preparation: A series of homogenous boron-doped carbon coated $Li_3V_2(PO_4)_3$ (referred as LVP/C+B) composites were synthesized via a sol-gel method, critic acid and sodium tetraphenylborate ($NaBC_{24}H_{20}$), which were used as carbon source and boron source, were

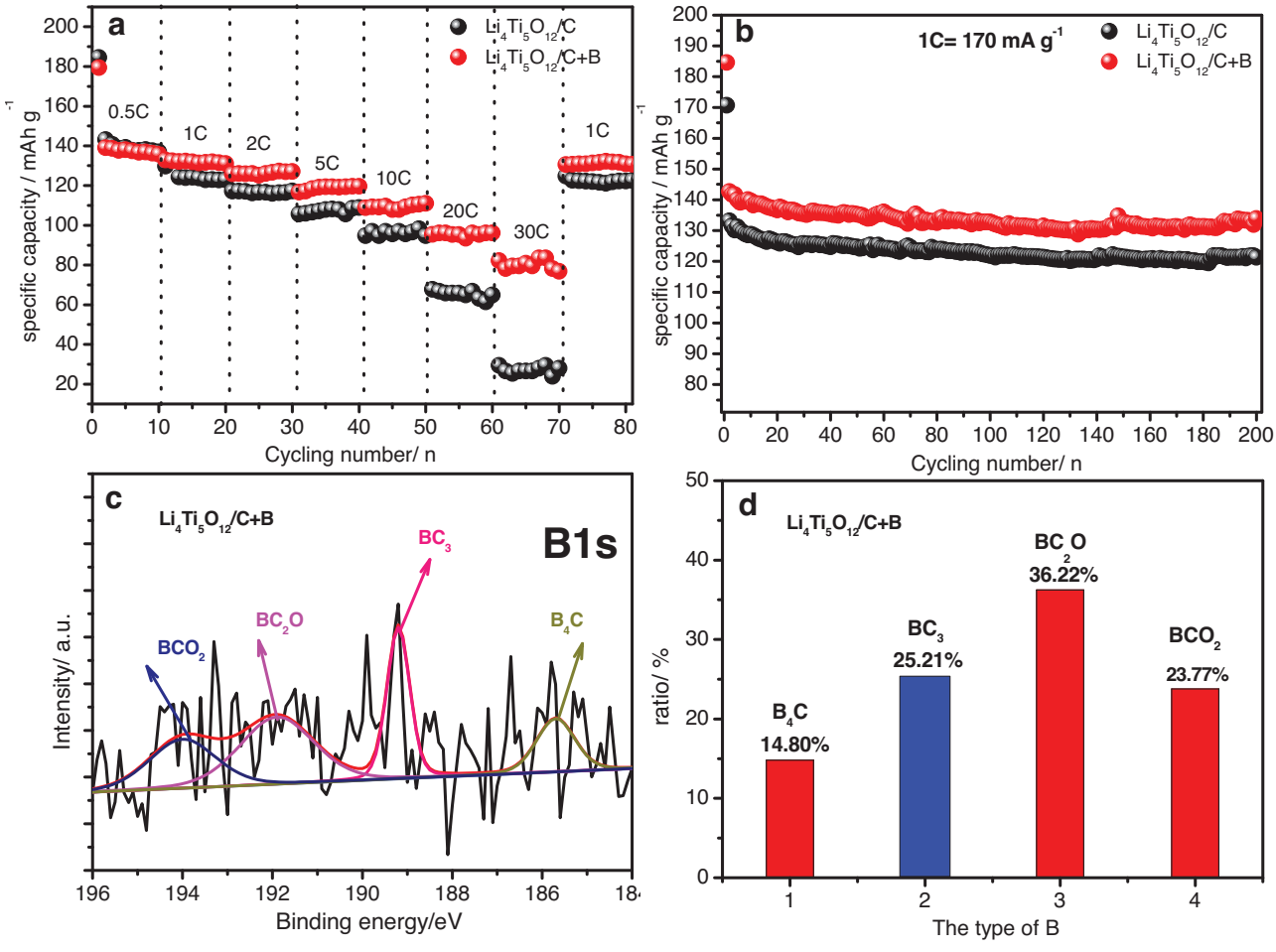

Figure 9. a) Rate performances and b) cycling performances of $Li_4Ti_5O_{12}$/C and $Li_4Ti_5O_{12}$/C+B samples in the potential range of 1.0–3.0 V; c) High-resolution XPS spectra of the $Li_4Ti_5O_{12}$/C+B on B1s; d) the ratio of different B types in each $Li_4Ti_5O_{12}$/C+B.

© 2014 WILEY-VCH Verlag GmbH & Co. KGaA, Weinheim

initially dissolved in distilled water with continuous stirring at room temperature. For preparation of LVP/C+B composites with different boron concentration, $NaBC_{24}H_{20}$ was added into the critic acid solution with different molar ratio to critic acid of 0, 0.33, 0.50, 0.67 and 0.83%, respectively. Then $LiOH{\cdot}H_2O$, V_2O_5 and H_3PO_4 (85%wt.) with the molar ratio of 3.05:1:3 were added into the above solutions in sequence under constantly stirring. The mixture was heated at 80 °C for several hours with vigorous stirring to evaporate the water until a green gel was generated. The obtained gel precursors were dried at 120 °C in a vacuum oven. The obtained powders were grinded and pre-heated at 300 °C for 4 h with following N_2. After cooling to room temperature, the resulting products were ground and sintered at 850 °C for 10 h in N_2 atmosphere to yield various $Li_3V_2(PO_4)_3$/C+B samples. $Li_3V_2(PO_4)_3$/C+B composites with different boron contents of 0, 0.33, 0.50, 0.67 and 0.83% are referred as LVP/C, LVPC-B33, LVPC-B50, LVPC-B67, LVPC-B83, respectively. Wherein, LVP/C is the bare carbon coated $Li_3V_2(PO_4)_3$ composite synthesized *via* the above-mentioned process except of the addition of $NaBC_{24}H_{20}$.

In order to further confirm and verify the modification effects of boron doped carbon coating, boron-doped carbon coated $Li_4Ti_5O_{12}$ material (referred as $Li_4Ti_5O_{12}$/C+B) was also prepared with sol-gel method. For preparation of $Li_4Ti_5O_{12}$/C+B, stoichiometric amounts of $Ti(C_4H_9O)_4$ (TBT) and Li_2CO_3 (5.0:2.1) was dissolved in ethanol-HNO_3 preblended solution in the volume ratio of TBT: ethanol:HNO_3 of 1:12:0.5. The necessary amount of EDTA and Citric acid (0.8:1.6), which were pre-dissolved in ammonia, were then gradually dropped into the mixed metal ion solution. A certain amount of $NaBC_{24}H_{20}$, with molar ratio to citric acid of 0.37%, was also dropped into the mixed metal ion solution. Then the mixed solution was slowly stirred for 12 h at 80 °C and finally turned into a transparent gel after drying. The resulting gelatin was heat-treated at 250 °C over 6 h in the air to extract out excess ethanol and yield a solid organic $Li_4Ti_5O_{12}$ precursor. The solidified precursor was pretreated by planetary ball milling for 10 h then sintered under N_2 atmosphere at 800 °C for 15 h to obtain final powders. The preparation process of the controlled carbon coated $Li_4Ti_5O_{12}$ sample (referred as $Li_4Ti_5O_{12}$/C) is identical to $Li_4Ti_5O_{12}$/C+B just without the addition of $NaBC_{24}H_{20}$.

Characterization: The X-ray diffraction patterns of various $Li_3V_2(PO_4)_3$/C+B and $Li_4Ti_5O_{12}$/C+B samples were determined by the D/max-Ultima III Diffractometer at 40 kV, 40 mA with Cu–Kα radiation (λ = 0.154 nm). The carbon contents of $Li_3V_2(PO_4)_3$/C and various $Li_3V_2(PO_4)_3$/C+B samples were measured by an organic element analyzer (Vario EL cube). The HRTEM images were observed using a high resolution transmission electron microscope (HR-TEM, Hitachi H-800). The Raman spectra were achieved on a labRAM ARAMIS laser Raman spectroscopy equipped with a 514 nm Ar-ion laser. The XPS spectra were performed on a PHI Quantera SXM scanning X-ray microprobe with 100 mm beam size, using an Al Kα (λ = 0.83 nm, hυ = 1486.7 eV) X-ray source operated at 2 kV and 20 mA. Power electronic conductivity investigation at the pressure of 4 MPa was performed on Powder Resistivity Meter (FZ-2010,Changbao Analysis Co., Ltd, Shanghai, China).

Electrochemical Tests: Electrochemical performances of various $Li_3V_2(PO_4)_3$/C+B and $Li_4Ti_5O_{12}$/C+B composites were investigated using CR2032 coin-type cell. A metallic lithium foil served as the reference and counter electrode. The work electrodes were fabricated with active material, acetylene black and polyvinylidene difluoride (PVDF) at a weight ratio of 80:10:10. The slurry of $Li_3V_2(PO_4)_3$ was pasted onto the Al foil and the slurry of $Li_4Ti_5O_{12}$ was pasted onto the Cu foil, these electrodes were dried at 120 °C in vacuum for 12 h. The cells were assembled in an argon filled glove box. The mass loading of each electrode plate was around 2.0–2.5 mg cm^{-2}. 1M $LiPF_6$ in ethylene carbonate (EC)/dimethyl carbonate (DMC) /ethylene methyl carbonate (EMC) with the volumetric ratio of 1:1:1 as the electrolyte, and a polypropylene micro-porous film (Cell-gard 2300) as the separator. The galvanostatic charge-discharge tests were conducted on LAND CT2001A test system (Wuhan, China). All the tests were performed in the potential ranges of 3.0–4.3 V and 3.0–4.8 V for $Li_3V_2(PO_4)_3$, and 1.0–3.0 V for $Li_4Ti_5O_{12}$. Electrochemical impedance spectroscopy tests were conducted on a Zahner IM6e Electrochemical Workstation with frequency of 1 MHz to 10 mHz at the full charge state (4.3 V) after the 50th and 100th cycle.

Supporting Information

Supporting Information is available from the Wiley Online Library or from the author.

Acknowledgements

This work was financially supported by the National Nature Science Foundation of China (No. 51102010,21336003, 21371021), the Fundamental Research Funds for the Central Universities (Grant No. ZZ1232), the Program for New Century Excellent Talents in University of China (NCET-12–0758).

Received: March 29, 2014
Revised: April 25, 2014
Published online: July 3, 2014

[1] H. Li, H. S. Zhou, *Chem. Commun.* **2012**, *48*, 1201.
[2] M. Gaberscek, R. Dominko, J. Jamnik, *Electrochem. Commun.* **2007**, *9*, 2778.
[3] Y. G. Wang, H. Li, P. He, E. Hosono, H. S. Zhou, *Nanoscale* **2010**, *2*, 1294.
[4] Y. G. Wang, Y. Wang, E. Hosono, K. Wang, H. S. Zhou, *Angew. Chem. Int. Ed.* **2008**, *47*, 7461.
[5] X. Liu, P. Yan, Y. Y. Xie, H. Yang, X. Shen, Z. F. Ma, *Chem. Commun.* **2013**, *49*, 5396.
[6] W. Mao, J. Yan, H. Xie, Z. Tang, Q. Xu, *Electrochim. Acta* **2013**, *88*, 429.
[7] W. Yuan, J. Yan, Z. Tang, O. Sha, J. Wang, W. Mao, L. Ma, *J. Power Sources* **2012**, *201*, 301.
[8] Y. G. Wang, H. Liu, K. Wang, H. Eiji, Y. Wang, H. S. Zhou, *J. Mater. Chem.* **2010**, *20*, 595.
[9] J. Song, T. Xu, M. L. Gordin, P. Zhu, D. Lv, Y. B. Jiang, Y. Chen, Y. Duan, D. Wang, *Adv. Funct. Mater.* **2014**, *24*, 1243.
[10] E. Yoo, J. Nakamura, H. S. Zhou, *Energy Environ. Sci.* **2012**, *5*, 6928.
[11] Y. Zhao, L. Yang, S. Chen, X. Wang, Y. Ma, Q. Wu, Y. Jiang, W. Qian, Z. Hu, *J. Am. Chem. Soc.* **2013**, *135*, 1201.
[12] Z. S. Wu, A. Winter, L. Chen, Y. Sun, A. Turchanin, X. L. Feng, K. Mullen, *Adv. Mater.* **2012**, *24*, 5130.
[13] Z. S. Wu, W. Ren, L. Xu, F. Li, H. M. Cheng, *ACS Nano* **2011**, *5*, 5463.
[14] R. Yi, J. Zai, F. Dai, M. L. Gordin, D. Wang, *Electrochem. Commun.* **2013**, *36*, 29.
[15] L. Zhao, Y. S. Hu, H. Li, Z. X. Wang, L. Q. Chen, *Adv. Mater.* **2011**, *23*, 1385.
[16] S. Yoon, C. Liao, X. G. Sun, C. A. Bridges, R. R. Unocic, J. Nanda, S. Dai, M. P. Paranthaman, *J. Mater. Chem.* **2012**, *22*, 4611.
[17] C. Wang, W. Shen, H. M. Liu, *New J. Chem.* **2014**, *38*, 430.
[18] J. Han, L. L. Zhang, S. Lee, J. Oh, K. S. Lee, J. R. Potts, J. Ji, X. Zhao, R. S. Ruoff, S. Park, *ACS Nano* **2013**, *7*, 19.
[19] L. S. Panchakarla, K. S. Subrahmanyam, S. K. Saha, A. Govindaraj, H. R. Krishnamurthy, U. V. Waghmare, C. N. R. Rao, *Adv. Mater.* **2009**, *21*, 4726.
[20] Y. A. Kim, K. Fujisawa, H. Muramatsu, T. Hayashi, M. Endo, T. Fujimori, K. Kaneko, M. Terrones, J. Behrends, A. Eckmann, C. Casiraghi, K. S. Novoselov, R. Saito, M. S. Dresselhaus, *ACS Nano* **2012**, *6*, 6293.
[21] C. Wang, H. M. Liu, W. S. Yang, *J. Mater. Chem.* **2012**, *22*, 5281.

© 2014 WILEY-VCH Verlag GmbH & Co. KGaA, Weinheim

[22] L. Yang, S. Jiang, Y. Zhao, L. Zhu, S. Chen, X. Wang, Q. Wu, J. Ma, Y. Ma, Z. Hu, *Angew. Chem. Int. Ed.* **2011**, *50*, 7132.
[23] M. Cattelan, S. Agnoli, M. Favaro, D. Garoli, F. Romanato, M. Meneghetti, A. Barinov, P. Dudin, G. Granozzi, *Chem. Mater.* **2013**, *25*, 1490.
[24] Y. Li, J. Wang, X. Li, D. Geng, M. N. Banis, R. Li, X. Sun, *Electrochem. Commun.* **2012**, *18*, 12.
[25] S. Wang, E. Iyyamperumal, A. Roy, Y. Xue, D. Yu, L. Dai, *Angew. Chem. Int. Ed.* **2011**, *50*, 11756.
[26] Y. B. Tang, L. C. Yin, Y. Yang, X. H. Bo, Y. L. Cao, H. E. Wang, W. J. Zhang, I. Bello, S. T. Lee, H. M. Cheng, C. S. Lee, *ACS Nano* **2013**, *6*, 1970.
[27] G. Jo, S. Shanmugam, *Electrochem. Commun.* **2012**, *25*, 101.
[28] J. Ozaki, N. Kimura, T. Anahara, A. Oya, *Carbon* **2007**, *45*, 1847.
[29] T. Kwon, H. Nishihara, H. Itoi, Q. H. Yang, T. Kyotani, *Langmuir* **2009**, *25*, 11961.
[30] S. C. Yin, H. Grondey, P. Strobel, H. Huang, L. F. Nazar, *J. Am. Chem. Soc.* **2003**, *125*, 326.
[31] H. Huang, S. C. Yin, T. Kerr, N. Taylor, L. F. Nazar, *Adv. Mater.* **2002**, *14*, 1525.
[32] T. Wu, H. Shen, L. Sun, B. Cheng, B. Liu, J. Shen, *New J. Chem.* **2012**, *36*, 1385.
[33] B. Zheng, P. Hermet, L. Henrard, *ACS Nano* **2010**, *4*, 4165.
[34] B. Guo, Q. Liu, E. Chen, H. Zhu, L. Fang, J. R. Gong, *Nano Lett.* **2010**, *10*, 4975.
[35] Z. S. Wu, W. Ren, L. Gao, J. Zhao, Z. Chen, B. Liu, D. Tang, B. Yu, C. Jiang, H. M. Cheng, *ACS Nano* **2009**, *3*, 411.
[36] I. Mukhopadhyay, N. Hoshino, S. Kawasaki, F. Okino, W. K. Hsu, H. Touhara, *J. Electrochem. Soc.* **2002**, *149*, A39.
[37] G. N. Zhu, H. J. Liu, J. H. Zhang, C. X. Wang, Y. G. Wang, Y. Y. Xia, *Energy Environ. Sci.* **2011**, *4*, 4016.
[38] C. Zhang, Y. Zhang, J. Wang, D. Wang, D. He, Y. Y. Xia, *J. Power Sources* **2013**, *236*, 118.

© 2014 WILEY-VCH Verlag GmbH & Co. KGaA, Weinheim